Quantum Spin Microscopy's Emerging Methods, Roadmaps, and Enterprises

John A. Sidles, Joseph L. Garbini, Jonathan P. Jacky, and Rico A. R. Picone
Quantum Systems Engineering Laboratory, University of Washington, Seattle, WA, USA

Presented as abstract #015, 52nd ENC, April 10–15 2011, Asilomar CA.

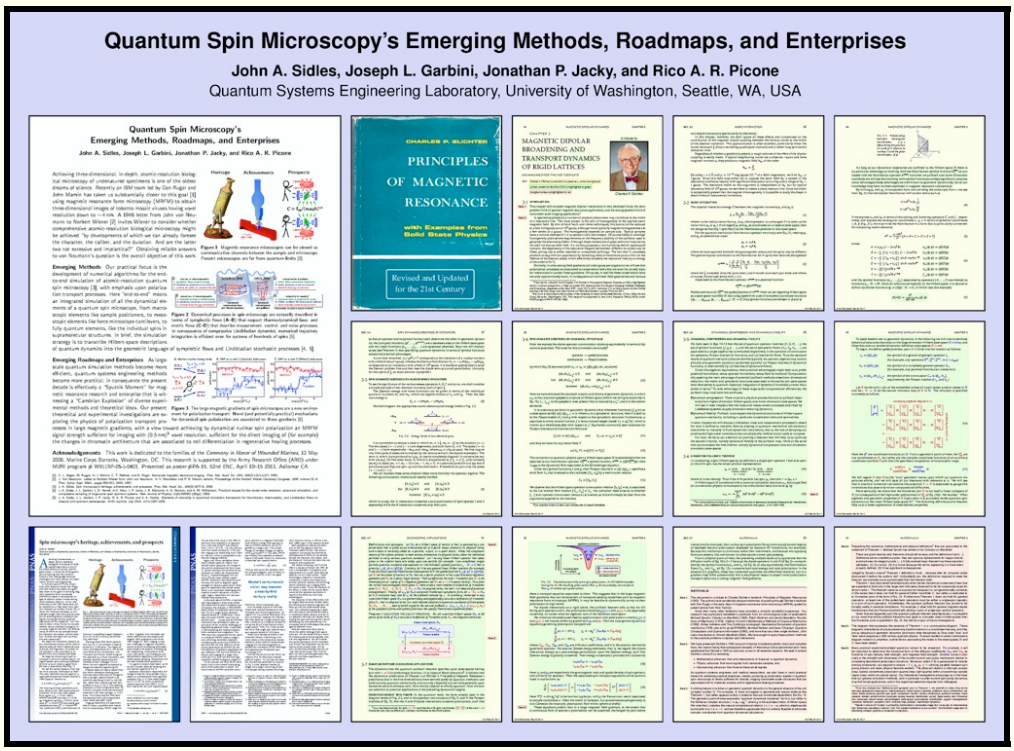

A tribute to Charles P. Slichter

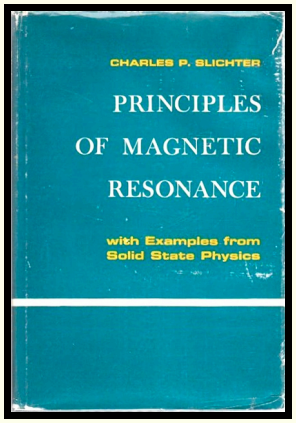

and his *Principles of Magnetic Resonance*

[1] On-line text and poster: **`http://faculty.washington.edu/sidles/ENC_2011/`**

[2] This work is dedicated to the families of the *Ceremony in Honor of Wounded Marines*, 12 May 2006, Marine Corps Barracks, Washington, DC. This research is supported by the Army Research Office (ARO) under MURI program # W911NF-05-1-0403. This version is v3.3x (final version, May 29, 2011), as amended to reflect conversations with ENC colleagues at Asilomar, and with Dan Rugar, and with John Marohn.

CHARLES P. SLICHTER

PRINCIPLES OF MAGNETIC RESONANCE

with Examples from Solid State Physics

Revised and Updated for the 21st Century

CHAPTER 3

MAGNETIC DIPOLAR BROADENING AND TRANSPORT DYNAMICS OF RIGID LATTICES

(AS IMAGINED FOR THE 21ST CENTURY)

A tribute to

Charles P. Slichter

KEY: Slichter's 1963 text (verbatim) is typeset on a yellow background

added content for the 52nd ENC is highlighted in green

marginal notes are highlighted in red

3.1 INTRODUCTION

Note 1 This chapter will consider magnetic dipolar interactions in two idealized limits: the zero-gradient limit of spectral magnetic resonance applications, and the strong-gradient limit of nanometer-scale imaging applications.[1]

Note 2 In spectral applications a number of physical phenomena may contribute to the width of a resonance line. The most prosaic is the lack of homogeneity of the applied static magnetic field. By dint of hard work and clever techniques, this source can be reduced to a few milligauss out of 10^4 gauss, although more typically magnet homogeneities are a few tenths of a gauss. The homogeneity depends on sample size. Typical samples have a volume between 0.1 cc to several cubic centimeters. Of course fields of ultrahigh homogeneity place severe requirements on the frequency stability of the oscillator used to generate the alternating fields. Although these matters are of great technical importance, we shall not discuss them here. If a nucleus possesses a non-vanishing electric quadrupole moment, the degeneracy of the resonance frequencies between different m-values may be lifted, giving rise to either resolved or unresolved splittings. The fact that T_1 processes produce an equilibrium population by balancing rates of transitions puts a limit on the lifetime of the Zeeman states, which effectively broadens the resonance lines by an energy of the order of $\hbar/T_1$.

Similarly, in ultra-strong field gradients (of order gauss per angstrom) we will see that polarization processes are associated to conservation laws that are exact for purely dipolar interactions in purely linear gradients. Of course, in real life these conservation laws are only approximately exact, in consequence of nonlinear field geometries and various

[1] Plain text is verbatim from Chapter 3 of Slichter's *Principles of Magnetic Resonance* (1963); highlighted text is a modern perspective, written for poster 015, *Quantum Spin Microscopy's Emerging Methods, Roadmaps, and Enterprises*, presented at the 52nd ENC, April 10–15, 2011, Asilomar CA, on the occasion of John Sidles sharing with Dan Rugar and John Mamin (of IBM) the Günther Laukien Prize for 2011.

This work is dedicated to the families of the *Ceremony in Honor of Wounded Marines*, 12 May 2006, Marine Corps Barracks, Washington, DC. This research is supported by the Army Research Office (ARO) under MURI program #W911NF-05-1-0403.

non-dipole interactions (particularly for electrons).

In this chapter, however, we shall ignore all these effects and concentrate on the contribution of the magnetic dipole coupling between the various nuclei to the width of the Zeeman transition. This approximation is often excellent, particularly when the nuclei have spin $\frac{1}{2}$ (thus a vanishing quadrupole moment) and a rather long spin-lattice relaxation time.

Regardless of whether a gradient is present, a rough estimate of the effect of the dipolar coupling is easily made. If typical neighboring nuclei are a distance r apart and have magnetic moment μ, they produce a magnetic field H_{loc} of the order

$$\mathsf{H}_{\text{loc}} = \frac{\mu}{r^3}$$

By using $r = 2\,\text{Å}$ and $\mu = 10^{-23}$ erg/gauss (10^{-3} of a Bohr magneton), we find $\mathsf{H}_{\text{loc}} \simeq 1\,\text{gauss}$. Since this field may either aid or oppose the static field H_0, a spread in the resonance conditions results, with significant absorption occurring over a range of $\mathsf{H}_0 \sim 1$ gauss. The resonance width on this argument is independent of H_0, but for typical laboratory field of 10^4 gauss, we see there is indeed a sharp resonant line. Since the width is substantially greater than the magnet inhomogeneity, it is possible to study the shape in detail without instrumental limitations.

3.2 BASIC INTERACTION

The classical interaction energy E between two magnetic moments $\boldsymbol{\mu}_1$ and $\boldsymbol{\mu}_2$ is

$$E = \frac{\boldsymbol{\mu}_1 \cdot \boldsymbol{\mu}_2}{r^3} - \frac{3(\boldsymbol{\mu}_1 \cdot \boldsymbol{r})(\boldsymbol{\mu}_2 \cdot \boldsymbol{r})}{r^5} \tag{1}$$

where $\boldsymbol{r}$ is the radius vector from $\boldsymbol{\mu}_1$ to $\boldsymbol{\mu}_2$ (the expression is unchanged if $\boldsymbol{r}$ is taken as the vector from $\boldsymbol{\mu}_2$ to $\boldsymbol{\mu}_1$.) If we regard $\boldsymbol{\mu}_1$ and $\boldsymbol{\mu}_2$ as coordinates on a classical state-space, then we recognize that Eq. 1 specifies E as the *Hamiltonian potential* on that state-space.

For the quantum mechanical Hamiltonian operator we simply take Eq. (1), treating $\boldsymbol{\mu}_1$ and $\boldsymbol{\mu}_2$ as operators as usual:

$$\begin{aligned} \boldsymbol{\mu}_1 &= \gamma_1 \hbar\, \mathbf{I}_1 \\ \boldsymbol{\mu}_2 &= \gamma_2 \hbar\, \mathbf{I}_2 \end{aligned} \tag{2}$$

where we have assumed that both the gyromagnetic rations and the spins may be different. The general dipolar contribution to the Hamiltonian for N spins then becomes the operator

$$H^{\text{dipole}} = \frac{1}{2} \sum_{j=1}^{N} \sum_{k=1}^{N} \left[\frac{\boldsymbol{\mu}_k \cdot \boldsymbol{\mu}_j}{r_{jk}^3} - \frac{3(\boldsymbol{\mu}_1 \cdot \boldsymbol{r}_{jk})(\boldsymbol{\mu}_2 \cdot \boldsymbol{r}_{jk})}{r_{jk}^5} \right] \tag{3}$$

where the $\frac{1}{2}$ is needed, since the sums over j and k would count each pair twise and where, of course, we exclude terms with $j = k$.

Associated to the Hamiltonian operator H^{dipole} is a potential function

$$h_{\mathcal{H}}^{\text{dipole}} = \langle \bar{\psi} | H^{\text{dipole}} | \psi \rangle$$

Mathematicians call $h_{\mathcal{H}}^{\text{dipole}}$ the *symbol function* of H^{dipole}. Here we are regarding Hibert space as a state-space manifold $\mathcal{H}$ that is equipped with a set of (complex) coordinate functions $(\psi_1, \ldots, \psi_{\dim \mathcal{H}}, \bar{\psi}_1, \ldots, \bar{\psi}_{\dim \mathcal{H}}) \colon \mathcal{H} \to \mathbb{C}$; thus symbol functions are *bilinear* in $\bar{\psi}$ and ψ.

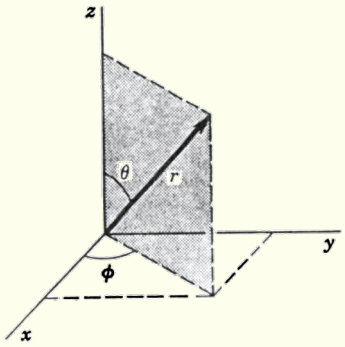

FIG. 3.1. Relationship between rectangular coordinates x, y, z (describing the position of nucleus 2 relative to nucleus 1) and the polar coordinates r, θ, ϕ.

As long as our dynamical trajectories are confined to the Hilbert space $\mathcal{H}$ there is no particular advantage to working with the Hamiltonian symbol function $h^{\text{dipole}}_{\mathcal{H}}$ as contrasted with the Hamiltonian operator H^{dipole}, but when we pullback onto lower-dimension manifolds we will see that working with symbol functions conveys significant computational advantages (these advantages are well-known to geometric dynamicists, but to our knowledge they have not been exploited in magnetic resonance calculations).

By writing $\boldsymbol{\mu}_1$ and $\boldsymbol{\mu}_2$ in component form and omitting the subscripts from r, we see from Eq. (1) that the dipolar Hamiltonian will contain terms such as

$$\begin{aligned} &\gamma_1\gamma_2\hbar^2\, \mathsf{I}_{1z}\mathsf{I}_{2z}\,\frac{1}{r^3} \\ &\gamma_1\gamma_2\hbar^2\, \mathsf{I}_{1z}\mathsf{I}_{2z}\,\frac{xy}{r^5} \end{aligned} \tag{4}$$

If we express I_{1z} and I_{2z} in terms of the raising and lowering operators I_1^+ and I_1^-, respectively, and express the rectangular coordinates x, y, z in terms of spherical coordinates r, θ, ϕ (Fig. 3.1), we may write the Hamiltonian in a form that is particularly convenient for computing matrix elements:

$$H^d = \frac{\gamma_1\gamma 2\hbar^2}{r^3}[A + B + C + D + E + F] \tag{5}$$

where

$$\begin{aligned} A &= \mathsf{I}_{1z}\mathsf{I}_{2z}\,(1 - 3\cos^2\theta) & a_{\mathcal{H}}(\bar\psi,\psi) &= \langle\bar\psi|A|\psi\rangle \\ B &= -\tfrac{1}{4}\left[\mathsf{I}_1^+\mathsf{I}_2^- + \mathsf{I}_1^-\mathsf{I}_2^+\right]\,(1 - 3\cos^2\theta) & b_{\mathcal{H}}(\bar\psi,\psi) &= \langle\bar\psi|B|\psi\rangle \\ C &= -\tfrac{3}{2}\left[\mathsf{I}_1^+\mathsf{I}_{2z} + \mathsf{I}_{1z}\mathsf{I}_2^+\right]\,\sin\theta\,\cos\theta\, e^{-i\phi} & c_{\mathcal{H}}(\bar\psi,\psi) &= \langle\bar\psi|C|\psi\rangle \\ D &= -\tfrac{3}{2}\left[\mathsf{I}_1^-\mathsf{I}_{2z} + \mathsf{I}_{1z}\mathsf{I}_2^-\right]\,\sin\theta\,\cos\theta\, e^{i\phi} & d_{\mathcal{H}}(\bar\psi,\psi) &= \langle\bar\psi|D|\psi\rangle \\ E &= -\tfrac{3}{4}\mathsf{I}_1^+\mathsf{I}_2^+ sin^2\theta\, e^{-2i\phi} & e_{\mathcal{H}}(\bar\psi,\psi) &= \langle\bar\psi|E|\psi\rangle \\ F &= -\tfrac{3}{4}\mathsf{I}_1^-\mathsf{I}_2^- sin^2\theta\, e^{+2i\phi} & f_{\mathcal{H}}(\bar\psi,\psi) &= \langle\bar\psi|F|\psi\rangle \end{aligned} \tag{6}$$

and the symbol functions $(a_{\mathcal{H}}, \ldots, f_{\mathcal{H}})$ associated to operators $(A, \ldots, F)$ are viewed as functions $a_{\mathcal{H}} : \mathcal{H} \to \mathbb{R}$. Given an orthonormal basis $|k\rangle$ on the Hilbert space, it is natural to define coordinate functions $\psi_k = \langle k|\psi\rangle : \mathcal{H} \to \mathbb{C}$, in which case (for example)

$$\langle k|A|l\rangle = \frac{\partial^2}{\partial\bar\psi^k\,\partial\psi^l}\, a_{\mathcal{H}}(\bar\psi,\psi) \tag{7}$$

so that an operator and its symbol function each determine the other. In geometric dynamics, the (complex) functions $(\psi^1, \ldots, \psi^{\dim \mathcal{H}})$ are a *coordinate atlas* on the Hilbert state-space and the (real) functions $(a_{\mathcal{H}}, \ldots, f_{\mathcal{H}}, \ldots)$ are *dynamical potentials*. Soon we will demonstrate (see Theorem 1) that specifying quantum dynamics in terms of symbol functions substantial practical advantages.

As we have remarked, $(\gamma_1\gamma_2\hbar^2)/r^3$ corresponds to the interaction of a nuclear moment with a field of about 1 gauss, whereas the Zeeman Hamiltonian $\mathsf{H}_Z = -\gamma_1\hbar\mathsf{H}_0\mathsf{I}_{1z} - \gamma_2\hbar\mathsf{H}_0\mathsf{I}_{2z}$ corresponds to an interaction with a field of 10^4 gauss. It is therefore appropriate to solve the Zeeman problem first and then treat the dipole term as a small perturbation. (Actually, for two spins of $\frac{1}{2}$, an exact solution is possible.)

3.3 SPIN DYNAMICS DESCRIBED BY HILBERT-SPACE OPERATORS

To see the significance of the various ~~terms~~ operators A, B, C and so on, we shall consider a simple example of two identical moments, both of spin $\frac{1}{2}$.

The Zeeman energy and wave functions can be given in terms of the individual quantum numbers m_1 and m_2, which are eigenfunctions of I_{1z} and I_{2z}. Then the Zeeman energy is

$$E_Z = -\gamma\hbar\mathsf{H}_0 m_1 - \gamma\hbar\mathsf{H}_0 m_2 \tag{8}$$

We shall diagram the appropriate matrix elements and energy levels in Fig. 3.2.

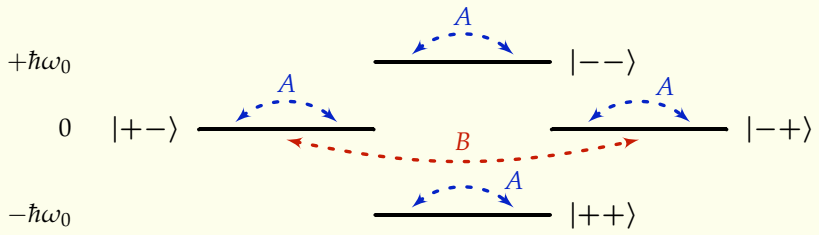

FIG. 3.2. Energy levels of two identical spins.

It is convenient to denote a state in which $m_1 = +\frac{1}{2}$, $m_2 = -\frac{1}{2}$ by the notation $(+-)$. The two states $|+-\rangle$ and $|-+\rangle$ are degenerate, and both have $E_Z = 0$. The states $|++\rangle$ and $|--\rangle$ have respectively $-\hbar\omega_0$ and $+\hbar\omega_0$, where $\omega_0 = \gamma\mathsf{H}_0$ as usual. We first inquire into what parts of states are connected by the various terms in the dipolar expression. The term A, which is proportional to $\mathsf{I}_{1z}\mathsf{I}_{2z}$, is clearly completely diagonal: it connects $|m_1 m_2\rangle$ with $\langle m_1 m_2|$. On the other hand, B, which is proportional to $\mathsf{I}_1^+\mathsf{I}_2^- + \mathsf{I}_1^-\mathsf{I}_2^+$, only connects $|m_1 m_2\rangle$ to states $\langle m_1 + 1, m_2 - 1|$ or $\langle m_1 - 1, m_2 + 1|$. A customary parlance is to say that B simultaneously flips one spin up and the other down. B therefore can join only the states $|+-\rangle$ and $|-+\rangle$.

We can express these same physical ideas more formally via operator algebra. The following commutation relations are readily verified:

$$\begin{aligned} & [A, \mathsf{I}_{1z}] = 0 \quad \text{and} \quad [A, \mathsf{I}_{2z}] = 0 \\ \text{but} \quad & [B, \mathsf{I}_{1z}] \neq 0 \quad \text{and} \quad [B, \mathsf{I}_{2z}] \neq 0 \\ & \text{however} \quad [B, \mathsf{I}_{1z} + \mathsf{I}_{2z}] = 0 \end{aligned} \tag{9}$$

which is to say, the A interaction conserves z-axis polarization of spin-species 1 and 2 separately, while the B interaction conserves only their sum.

3·4 SPIN DYNAMICS DESCRIBED BY DYNAMICAL POTENTIALS

Now we express the above operator commutation relations equivalently in terms of dynamical potentials. The rules for this conversion are simply[2]

$$\begin{aligned} \textit{operators} &\rightarrow \textit{symbol functions} \\ \textit{commutators} &\rightarrow \textit{Poisson brackets} \end{aligned}$$

by which Eq. (9) becomes (with $\mathsf{I}_{1z} \rightarrow i_{1z} = \langle\bar{\psi}|\mathsf{I}_{1z}|\psi\rangle$, *etc.*, as above)

$$\begin{aligned} & \langle da, di_{1z}\rangle_{\omega_{\mathcal{H}}^{-1}} = 0 \qquad \text{and} \qquad \langle da, di_{2z}\rangle_{\omega_{\mathcal{H}}^{-1}} = 0 \\ \text{but} \quad & \langle db, di_{1z}\rangle_{\omega_{\mathcal{H}}^{-1}} \neq 0 \qquad \text{and} \qquad \langle db, di_{1z}\rangle_{\omega_{\mathcal{H}}^{-1}} \neq 0 \\ & \text{however} \quad \langle db, di_{1z} + di_{2z}\rangle_{\omega_{\mathcal{H}}^{-1}} = 0 \end{aligned} \tag{10}$$

Here we have embraced the standard notation and idioms of geometric dynamics, in which $\omega_{\mathcal{H}}$ is the canonical *symplectic structure* of Hilbert space (which we will give explicitly in Eq. 15), $\langle\cdot,\cdot\rangle_{\omega_{\mathcal{H}}^{-1}}$ is the *symplectic inner product* that is induced by $\omega_{\mathcal{H}}^{-1}$, and d is the *exterior derivative*.

It is customary parlance in geometric dynamics that whenever functions (f, g, h) on a state-space satisfy $\langle df, dg\rangle_{\omega^{-1}} = h$, where ω is a symplectic structure, then h is said to be the *Poisson bracket* of f and g with respect to that symplectic structure. Furthermore, ω associates to every smooth function f a vector-valued *tangent bundle* $X_f = \phi_\omega^{-1} df$, which is known as a *Hamiltonian flow* with respect to f. Equivalent commonly seen notations for Poisson brackets and Hamiltonian flows are

$$\{f, d\} = \langle df, dg\rangle_{\omega^{-1}} \qquad \text{and} \qquad X_f \lrcorner\, \omega = i_{X_f}\omega = df \tag{11}$$

and thus we have for any vector field Y

$$\omega(X_f, Y) = df(Y) = Y(f) \tag{12}$$

The connection to quantum physics upon a Hilbert state-space $\mathcal{H}$ is established when we associate to our Hamiltonian operator $H_{\mathcal{H}}^{\text{dipole}}$ a symbol function, $h^{\text{dipole}} = \langle\bar{\psi}|H_{\mathcal{H}}^{\text{dipole}}|\psi\rangle$; then $X_{h^{\text{dipole}}}$ is the dynamical flow associated to the Schroedinger equation.

Given two symbol functions f and g, their Poisson bracket $h = \langle df, dg\rangle_{\omega^{-1}}$ specifies a third flow X_h that is related to the *Lie bracket* $[X_f, X_g]$ by a well-known relation

$$X_h = [X_g, X_f] \tag{13}$$

We observe that the Hilbert space operator commutation relation $[\mathsf{I}_x, \mathsf{I}_y] = \mathbb{i}\mathsf{I}_z$ is associated to the Lie bracket flow relation $[X_{i_x}, X_{i_y}] = X_{i_z}$. No confusion need arise as to whether $[\cdot,\cdot]$ is an operator commutator versus a Lie bracket, as this will always be clear from the arguments supplied to the brackets.

[2] Our notation is that of John Lee's *Introduction to Smooth Manifolds.*

3.5 DYNAMICAL COMPRESSION AND DYNAMICAL FIDELITY

We have seen in Eqs. 10–13 that the set of quantum operator matrices $(F, G, H, \ldots)$, the set of symbol functions $(f, g, h, \ldots)$, and the set of symplectic flows $(X_f, X_g, X_h, \ldots)$ are associated to a single algebra that is embodied respectively in the operation of commutator for operators, Poisson bracket for functions, and Lie bracket for flows. Thus the standard results of quantum mechanics (that are derived typically via operator algebra) map isomorphically onto geometric dynamics (as derived typically via Poisson brackets of dynamical functions, or alternatively by Lie brackets of dynamical flows).

Given this algebraic equivalence, what practical advantage(s) might lead us to prefer potential formalisms, *versus* operator formalisms, *versus* flow formalisms? Computationally speaking the main advantage of potential/pullback methods arises from dimensional reduction: the metric and symplectic structures associated to Kronecker join state-spaces lend themselves to quantum trajectory integration of systems of hundreds or even thousands of spins.[3] To take advantage of these large-scale computational efficiencies, the pullback map must have two attributes:

Dynamical compression There must be a physical process that acts to pullback trajectories from higher-dimension Hilbert spaces onto lower-dimension state-spaces. We will see in later chapters that the noise and measurement processes described by *Lindbladian dynamics* supply dimension-reducing dynamics.

Dynamical fidelity Pullback must respect the dynamical structures of Hilbert-space quantum mechanics, including in particular conservation laws and symmetries.

In later chapters we will discuss Lindbladian noise and measurement processes in detail; for now it suffices to conceive them as playing in quantum mechanical calculations a role similar to viscosity in fluid dynamical calculations, that is, the role of damping-out small-scale/high-order correlations that are physically irrelevant and costly to compute.

For now, we focus our attention on proving a theorem that will help us to optimize the second criterion, namely dynamical fidelity of the pullback map, while at the same time accommodate the first criterion, namely dynamical compression onto low-dimension simulation state-spaces.

3.6 A QUANTUM PULLBACK THEOREM

In considering n-spin Hilbert spaces, by definition a single-spin operator I that acts upon on the m'th spin has the tensor product representation

$$\mathsf{I}_m = \underbrace{\mathrm{id} \otimes \ldots \otimes \mathrm{id}}_{m-1 \text{ times}} \otimes I \otimes \underbrace{\mathrm{id} \otimes \ldots \otimes \mathrm{id}}_{n-m \text{ times}} \tag{14}$$

where id is the identity. Thus if the m'th particle has spin j_m, then $\dim I = 2j_m + 1$.

A Hilbert space $\mathcal{H}$ is endowed with a canonical symplectic structure $\omega_{\mathcal{H}}$ that is specified (in conventional physics normalization) via orthonormal basis functions ψ_k by

$$\omega_{\mathcal{H}} = -\mathbb{i} \sum_{k=1}^{\dim \mathcal{H}} \left[d\psi^k \otimes d\bar{\psi}^k - d\bar{\psi}^k \otimes d\psi^k \right] \tag{15}$$

Note 3

[3] For computational details, see *"Elements of naturality in dynamical simulation frameworks for Hamiltonian, thermostatic, and Lindbladian flows on classical and quantum state-spaces,"* arXiv:1007.1958.

To assist readers new to geometric dynamics, in the following we will color-code those dynamical structures that exist on the large-dimension Hilbert state-space $\mathcal{H}$ in blue, and those that exist on smaller-dimension Kählerian state-spaces $\mathcal{K}$ in red.

To begin, we define *symbol functions* upon $\mathcal{H}$ in Dirac bra-ket notation as follows:

$i_{\mathcal{H}} = \langle\bar{\psi}|\mathsf{I}_{\mathcal{H}}|\psi\rangle$ the symbol of a general single-spin operator $\mathsf{I}_{\mathcal{H}}$ (for example, any operators $\mathsf{I}_x^{(m)}, \mathsf{I}_y^{(m)}, \mathsf{I}_z^{(m)}\ ;\ m \in 1, n_{\text{spin}}$)

$h_{\mathcal{H}} = \langle\bar{\psi}|\mathsf{H}_{\mathcal{H}}|\psi\rangle$ the symbol of a completely general operator $\mathsf{H}_{\mathcal{H}}$ (for example, any pairwise Hamiltonian interaction)

$c_{\mathcal{H}} = \langle ds_{\mathcal{H}}, dh_{\mathcal{H}}\rangle_{\omega_{\mathcal{H}}^{-1}}$ the symbol of the commutator $C_{\mathcal{H}} \equiv \mathbb{i}[\mathsf{I}_{\mathcal{H}}, \mathsf{H}_{\mathcal{H}}]$, (equivalently, the Poisson bracket of $i_{\mathcal{H}}$ and $h_{\mathcal{H}}$)

Let $\mathcal{K}$ be the rank-r *join* of the embedded subset of n-spin tensor product states in $\mathcal{H}$ and let $\iota\colon \mathcal{K} \hookrightarrow \mathcal{H}$ be the natural inclusion map of $\mathcal{K}$ in $\mathcal{H}$. The inclusion is specified concretely as follows

$$\begin{bmatrix}\psi^1\\ \vdots\\ \psi^{n_\psi}\end{bmatrix} = \begin{bmatrix}{}^1\xi_1^1\\ \vdots\\ {}^1\xi_{m_1}^1\end{bmatrix} \otimes \begin{bmatrix}{}^1\xi_1^2\\ \vdots\\ {}^1\xi_{m_2}^2\end{bmatrix} \otimes \begin{bmatrix}{}^1\xi_1^3\\ \vdots\\ {}^1\xi_{m_3}^3\end{bmatrix} \otimes \ldots \otimes \begin{bmatrix}{}^1\xi_1^n\\ \vdots\\ {}^1\xi_{m_n}^n\end{bmatrix} \quad \text{(increasing algebraic degree } n \rightarrow\text{)}$$
$$+ \begin{bmatrix}{}^2\xi_1^1\\ \vdots\\ {}^2\xi_{m_1}^1\end{bmatrix} \otimes \begin{bmatrix}{}^2\xi_1^2\\ \vdots\\ {}^2\xi_{m_2}^2\end{bmatrix} \otimes \begin{bmatrix}{}^2\xi_1^3\\ \vdots\\ {}^2\xi_{m_3}^3\end{bmatrix} \otimes \ldots \otimes \begin{bmatrix}{}^2\xi_1^n\\ \vdots\\ {}^2\xi_{m_n}^n\end{bmatrix}$$
$$+ \ \ldots$$
$$+ \begin{bmatrix}{}^r\xi_1^1\\ \vdots\\ {}^r\xi_{m_1}^1\end{bmatrix} \otimes \begin{bmatrix}{}^r\xi_1^2\\ \vdots\\ {}^r\xi_{m_2}^2\end{bmatrix} \otimes \begin{bmatrix}{}^r\xi_1^3\\ \vdots\\ {}^r\xi_{m_3}^3\end{bmatrix} \otimes \ldots \otimes \begin{bmatrix}{}^r\xi_1^n\\ \vdots\\ {}^r\xi_{m_n}^n\end{bmatrix} \quad \text{(increasing join rank } r \rightarrow\text{)} \tag{16}$$

Here the ψ^k are coordinate functions on $\mathcal{H}$. From a geometric point of view, the ${}^l\xi_m^k$ are not coordinates on $\mathcal{K}$, but rather are the complex coordinate functions of an auxilliary coordinate manifold $\mathcal{C}$ such that (16) specifies a composition of holomorphic maps

$$\mathcal{C} \xrightarrow[\text{(surjective map)}]{\text{quotient } /\, \psi} \mathcal{K} \xrightarrow[\text{(injective map)}]{\text{immersion}} \mathcal{H} \tag{17}$$

We will regard $\mathcal{K}$ (not $\mathcal{C}$) as the "true" geometric venue upon which our quantum trajectories evolve, and we will state all our theorems with reference to it. We will see that in practical numerical calculations the surjection $\mathcal{C} \rightarrow \mathcal{K}$ is associated to gauge-like invariances that pose only minor computational difficulties.

More seriously, we notice that the Kronecker join $\mathcal{K}$ is not itself a linear subspace of $\mathcal{H}$ (in consequence of the high-order polynomials in ${}^l\xi_m^k$ of Eq. (16)). We wonder, "What algebraic and geometric properties of $\mathcal{K}$ might allow it to accurately render quantum spin dynamics on the linear Hilbert state-space $\mathcal{H}$?" The following definitions and theorem help us to a better appreciation of these desired properties.

Definitions and synopsis. *Let $\mathcal{H}_n$ be a Hilbert space of vectors ψ that is spanned by a preferred basis that is given as an orthonormal set of n-factor tensor products (in physical terms, such a basis is variously called an n-particle, n-spin, or n-qudit basis). Allow the component vectors of the n-factor product to have various dimensions (in physical terms, allow the individual particles to carry various quantum numbers). Let I be any linear Hilbert operator that when given in the n-factor basis acts solely upon one particle (for example, I can raise/lower single-particle quantum numbers) and associate to I the (bilinear) symbol function $i_{\mathcal{H}}\colon \mathcal{H}\to\mathbb{C}$ that is given by $i_{\mathcal{H}}(\bar\psi,\psi)=\langle\bar\psi|\mathsf{I}|\psi\rangle$. Similarly, let H be any general linear Hilbert operator (for example, H can be a multi-particle Hamiltonian) and associate to H the symbol function $h_{\mathcal{H}}(\bar\psi,\psi)=\langle\bar\psi|\mathsf{H}|\psi\rangle$. Let $\mathcal{K}_1$ be the subset of vectors in $\mathcal{H}_n$ that are n-factor products in the n-particle basis (algebraic geometers call $\mathcal{K}_1$ an n-factor Segre variety). Then by definition the rank-r Kronecker join $\mathcal{K}_r$ is the immersed join of r copies of $\mathcal{K}_1$ (algebraic geometers call $\mathcal{K}_r$ an $(r-1)$'th secant variety). Thus from the initial (non-entangled) state-space $\mathcal{K}_1$ there arises a rank-indexed stratification of Kronecker joins $\mathcal{K}_1\subseteq\mathcal{K}_2\subseteq\ldots\subseteq\mathcal{K}_r\subseteq\ldots\subseteq\mathcal{K}_\infty=\mathcal{H}_n$ (in physical terms, the rank r is a measure of quantum entanglement). Finally, let $\omega_{\mathcal{H}}$ be $\mathcal{H}_n$'s canonical (Kählerian) symplectic form, let $\iota_r\colon\mathcal{K}_r\hookrightarrow\mathcal{H}_n$ be $\mathcal{K}_r$'s inclusion map, and let ι_r^* be the pullback induced by ι_r. In summary, immersed in any n-particle Hilbert space $\mathcal{H}_n$ is a geometrically and algebraically natural stratification of Kronecker joins $\mathcal{K}_r$, that in physical terms is a rank-indexed classical-to-quantum succession of state-spaces $\mathcal{K}_1,\mathcal{K}_2,\ldots,\mathcal{K}_r,\ldots$, each of which supports the natural pullback $\iota_r^*\colon(\omega_{\mathcal{H}},i_{\mathcal{H}},h_{\mathcal{H}})\to(\omega_{\mathcal{K}},i_{\mathcal{K}},h_{\mathcal{K}})$ of the symplectic forms and symbol functions that specify Hamiltonian dynamical flows.*

Note 4

Theorem 1 (QUANTUM PULLBACK THEOREM). *For all n-particle Hilbert spaces $\mathcal{H}_n$, at all points of all ranks of $\mathcal{H}_n$'s natural stratification of Kronecker joins $\mathcal{K}_r$, this diagram commutes:*

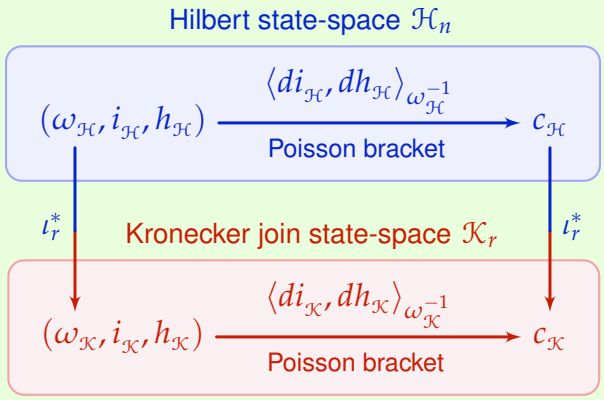

Note 5

3.7 QUANTUM SYSTEMS ENGINEERING APPLICATIONS

The dynamics that the quantum pullback theorem specifies upon state-spaces having join rank $r=0$ is comfortingly familiar—it is classical Bloch dynamics.[4] It follows that the dynamical predictions of Chapter 3 of Slichter's *Principles of Magnetic Resonance*—predictions that in the first three editions were derived solely by quantum methods—are valid not only quantum mechanically, and not only classically, but are valid generally upon Kronecker joins of arbitrary rank, from wholly classical to wholly quantum. Now we turn our attention to practical applications of the preceding dynamical insights.

COUNTER-CURRENT SPIN PUMPS At the quantum level, we have already seen in the diagram levels of Fig. 3.2, and in the operator commutators of Eq. 9, and in the Poisson brackets of Eq. 10, that the A and B dipole interactions conserve polarization, such that

[4] As a concrete example, for spin $j=1/2$ particles the m'th-spin coordinates $({}^1\xi_1^m,{}^1\xi_2^m)$ of the rank $r=0$ Kronecker join (16) are effectively complex coordinates on the Bloch sphere.

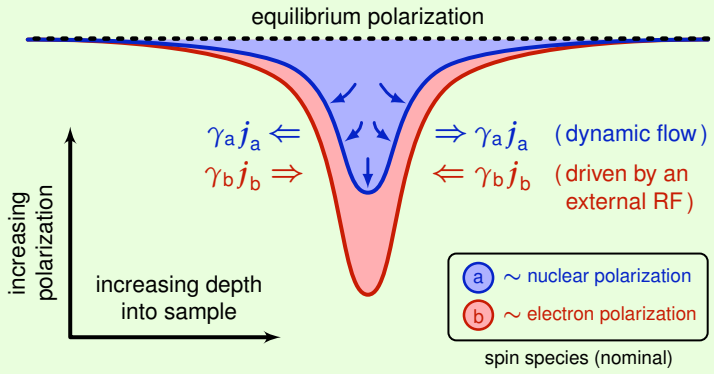

FIG. 3.3. The mechanism of dynamic spin polarization. An RF field drives electron spins (b); the resulting polarization flow j_b drives a steady, accumulative flow j_a of nuclear spin polarization.

there a transport equation associated to them. This suggests that in the large magnetic field gradients that are characteristic of nanoscale sensing modalities such as magnetic resonance force microscopy (MRFM), it may be feasible to dynamically pump nuclear polarization to high levels.

For dipole interactions on a rigid lattice, the pullback theorem tells us that for differing spin species a and b, the polarization densities $p_a(x,t)$ and $p_b(x,t)$ are separately conserved, no matter what the algebraic rank of the Kählerian state-space.

We introduce the *locality and linearity* approximation that polarization currents $j_a(x,t)$ and $j_b(x,t)$ are linearly driven by gradients of p_a and p_b. Then the most general dynamical equations governing polarization transport are

$$\frac{\partial}{\partial t} p_a = -\operatorname{div} j_a \qquad j_a = -\phi_g^{-1}\left[D_{aa}\, dp_a + D_{ab}\, dp_b\right]$$
$$\frac{\partial}{\partial t} p_b = -\operatorname{div} j_b \qquad j_b = -\phi_g^{-1}\left[D_{ba}\, dp_a + D_{bb}\, dp_b\right]$$

where D_{aa}, D_{ba}, D_{bb}, and D_{ab} are diffusion coefficients, and d is the exterior derivative (gradient) operator. We assume *Zeeman energy dominance*, that is, we regard the dipole interaction energy as a zero-average perturbation upon the Zeeman energy, such that Zeeman energy is globally conserved. Then energy conservation provides two constraints:

$$\begin{aligned} \gamma_b \rho_b D_{ba} &= -\gamma_a \rho_a D_{aa} \\ \gamma_a \rho_a D_{ab} &= -\gamma_b \rho_b D_{bb} \end{aligned} \tag{18}$$

Here γ_a and ρ_a are respectively the gyromagnetic ratio and spatial density of spin species a, and similarly for species b. Then the associated spin transport equations can be summarized in matrix form as:

$$\frac{\partial}{\partial t}\begin{bmatrix} \gamma_a \rho_a\, p_a(x,t) \\ \gamma_b \rho_b\, p_b(x,t) \end{bmatrix} = \begin{bmatrix} +\gamma_a \rho_a\, D_{aa} & -\gamma_b \rho_b\, D_{bb} \\ -\gamma_a \rho_a\, D_{aa} & +\gamma_b \rho_b\, D_{bb} \end{bmatrix} \nabla^2 \begin{bmatrix} p_a(x,t) \\ p_b(x,t) \end{bmatrix} \tag{19}$$

Here $\nabla^2 f = \operatorname{div} \phi_g^{-1} df$ is the familiar Laplacian, with g the Riemannian metric associated to sample coordinates x. Often the metric is Cartesian, but sometimes sample geometry is non-Cartesian (for example, polarization flow within spherical shells)

Note 6

These equations predict that in a large magnetic field gradient, to the extent that a continuous flow of species b polarization can be sustained (recharged by spin-lattice

interactions for example), then nuclear spin polarization flows continuously toward regions of depleted electron polarization (depleted by resonant RF interactions, for example). Because this mechanism is continuous rather than intermittent, and because two opposing flows are present, this mechanism is called *counter-current spin pumping*.

From a physical point of view, the preceding analysis leads us to appreciate that the diffusion matrix of Eq. 18 is 2×2 because the dipole operators A and B (of Eq. 5)—or equivalently, the symbol functions $a_{\mathcal{H}}$ and $b_{\mathcal{H}}$ (of Eq. 6), or also equivalently, the Hamiltonian flows $X_{a_{\mathcal{H}}}$ and $X_{b_{\mathcal{H}}}$ (of Eq. 13)—conserve both total energy and total polarization. In the absence of a gradient, these two conserved quantities are effectively identical, but in a gradient they differ substantially; this is the physical reason to expect novel polarization transport dynamics in strong magnetic field gradients.

MARGINALIA

Note 1: This document is a tribute to Charles Slichter's textbook *Principles of Magnetic Resonance* (1963). The authors have wonderfully pleasant memories of puzzling through Slichter's textbook with Dan Rugar in the early days of magnetic resonance force microscopy (MRFM), guided by patient advice from Nino Yannoni.

Since then many other textbooks have provided a similarly wonderful experience. Our research has particularly benefited in particular from (in chronological order of publication) Michael Spivak's *Calculus on Manifolds* (1965), Ralph Abraham and Jerrold Marsden's *Foundations of Mechanics* (1978), Vladimir Arnol'd's *Mathematical Methods of Classical Mechanics* (1998), Abhay Ashtekar and Troy Schilling's monograph *Geometrical formulation of quantum mechanics* (1999, see arXiv:gr-qc/9706069), Michael Nielsen and Isaac Chuang's *Quantum Computation and Quantum Information* (2000), and more than any other single textbook, John Lee's *Introduction to Smooth Manifolds* (2000). We have sought to apply these authors' methods to the practical problems of dipolar spin interactions.

Note 2: We have preserved Slichter's 1963 account of dipolar broadening wholly intact and complete here, the reason being that subsequent decades of theoretical and experimental work have established that Slichter's 1963 account was correct in all essential respects. We seek to extend Slichter's account by reviewing:

- *Mathematical advances* that unify descriptions of classical *vs* quantum dynamics,
- *Physics advances* that boost signals from nanoscale samples, and
- *Nanosensing advances* that observe these small signals.

As quantum systems engineers and medical researchers, we also have in mind practical means for achieving practical objectives, namely, pumping-up polarization signals in quantum spin microscopy to levels sufficient for directly imaging nanometer-scale structures that are associated both to materials science and to regenerative healing processes.

Note 3: A striking feature of articles on geometric quantum dynamics is the general absence of the unit complex number "$\mathbb{i}$." For example, "$\mathbb{i}$" does not appear in geometrically natural relations like Theorem 1, but rather appears solely in relations that are coordinate-dependent, like Eq. 15. The geometric point-of-view associates "quantum dynamical mysteries" not to $\mathbb{i}$, but rather to the Kählerian complex structure $J = \phi_\omega \circ \phi_g^{-1}$, where g is the euclidean metric of Hilbert space. We note that J satisfies the natural compositional relation $J \circ J = -\mathrm{id}$, which is algebraically isomorphic to $\mathbb{i} \times \mathbb{i} = -1$, and we therefore appreciate that it is entirely feasible to eliminate complex coordinates from quantum dynamical calculations.

Note 4: Regarding the numerous mathematical and physical definitions[5] that are associated to the statement of Theorem 1, Michael Spivak has written in his *Calculus on Manifolds*:

> There are good reasons why theorems should all be easy and the definitions hard [...] Definitions serve a twofold purpose: they are rigorous replacements for vague notions, and machinery for elegant proofs. [...] A fully evolved major theorem has three important attributes: (1) It is trivial. (2) It is trivial because the terms appearing in it have been properly defined. (3) It has significant consequences.

Judged by Spivak's criteria,[6] Theorem 1 definitely is trivial ... because after all, computer codes discovered it before the authors did! Undoubtedly too, the definitions required to state the theorem are markedly more sophisticated than the theorem itself.

Theorem 1 was discovered serendipitously when certain dynamical conservation laws that we expected to hold only in the large-rank limit were observed to be be numerically exact for all join ranks r. The theorem came as a surprise too because it is *not* geometrically universal, in the sense that it does *not* hold for general Kähler manifolds $\mathcal{K}$, but rather is restricted to to Kronecker joins of the form of Eq. 16. Furthermore Theorem 1 does *not* hold for general operators; at least one of the pulled-back operators must be either a single-spin operator, or a sum of such operators. Nonetheless, the quantum pullback theorem has proved to be broadly useful in practical simulations. For example, it *does* hold for general magnetic-dipole Hamiltonians that are Poisson-bracked with arbitrary sums of single-spin symbol operators.

Given that we happened upon the quantum pullback theorem serendipitously, it is plausible (in our view) that similar pullback theorems may apply to a broader class of state-spaces than the Kronecker joins is specified in Eq. 16; this will be a topic of future investigations.

Note 5: The diagram that expresses the essence of Theorem 1 is a *commutative diagram*. These diagrams characterize structure-preserving transformations in a coordinate-free way, and they are as ubiquitous in geometric dynamics (and many other disciplines) as Dirac-style "bras" and "kets" were ubiquitous in 20th century quantum physics. To assist readers to whom commutative diagram notation is unfamiliar, outline blocks associating the nodes to the state-spaces $\mathcal{H}$ and $\mathcal{K}$ have been added.

Note 6: Many practical experiment-related questions remain to be answered. For example, it will be important to determine the functional form of the diffusion coefficients D_{aa} and D_{bb} as functions of spin density, field strength, and magnetic field strength. Another concern obviously is the strength and robustness of the counter-current spin pump mechanism relative to competing decoherent polarization dynamics. Moreover, when (19) is generalized to include entropy constraints—as required to ensure $-1 \leq p_a, p_b \leq 1$—striking parallels between spin pump physics and laser physics become evident. The physical intuition is that spin pumps (resp. lasers) concentrate polarization quanta (resp. light quanta) within a low-entropy sample region (resp. within an optical cavity). Our theoretical investigations encourage us in the hope that our general simulation methods, and in particular counter-current spin pump dynamics, may find broad applications, and in this regard we welcome inquiries from colleagues.

---

[5] From the nineteen-line "definitions and synopsis" prior to Theorem 1, we read-off (in order) forty terms that have specialized meanings for mathematicians: *Hilbert space, spanned, preferred, basis, orthonormal, set, factor, tensor products, particle, spin, qudit, component, vectors, various, dimensions, quantum numbers, linear operator, bilinear, symbol function, associate, raising, lowering, Hamiltonian, subset, Segre variety, rank, Kronecker join, immersed, secant variety, non-entangled, state-space, rank-indexed, stratification, support, entanglement, canonical, Kahlerian, symplectic form, inclusion map, pullback, Hamiltonian dynamics*.

[6] Spivak's criterion of "triviality" is echoed by Grothendieck's memorable image of a "rising sea" of understanding that "advances insensibly in silence" until "the resistant substance is surrounded." Grothendieck's approach to describing complex systems is congenial to engineers.

Quantum Spin Microscopy's Emerging Methods, Roadmaps, and Enterprises

John A. Sidles, Joseph L. Garbini, Jonathan P. Jacky, and Rico A. R. Picone
Quantum Systems Engineering Laboratory, University of Washington, Seattle, WA, USA

Achieving three-dimensional, in-depth, atomic-resolution biological microscopy of undenatured specimens is one of the oldest dreams of science. Recently an IBM team led by Dan Rugar and John Mamin has taken us substantially closer to this goal [1] using magnetic resonance force microscopy (MRFM) to obtain three-dimensional images of tobacco mosaic viruses having voxel resolution down to $\sim 4\,\mathrm{nm}$. A 1946 letter from John von Neumann to Norbert Wiener [2] invites Wiener to consider whether comprehensive atomic-resolution biological microscopy might be achieved "by developments of which we can already foresee the character, the caliber, and the duration. And are the latter two not excessive and impractical?" Obtaining reliable answers to von Neumann's question is the overall objective of this work.

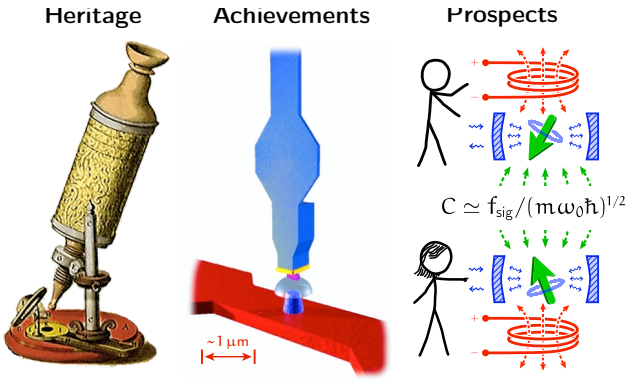

Figure 1 Magnetic resonance microscopes can be viewed as communication channels between the sample and microscope. Present microscopes are far from quantum limits [3].

Emerging Methods Our practical focus is the development of numerical algorithms for the end-to-end simulation of atomic-resolution quantum spin microscopy [3], with emphasis upon polarization transport processes. Here "end-to-end" means an integrated simulation of all the dynamical elements of a quantum spin microscope, from macroscopic elements like sample positioners, to mesoscopic elements like force microscope cantilevers, to fully quantum elements, like the individual spins in supramolecular structures. In brief, the simulation strategy is to transcribe Hilbert-space descriptions of quantum dynamics into the geometric language of symplectic flows and Lindbladian stochastic processes [4, 5].

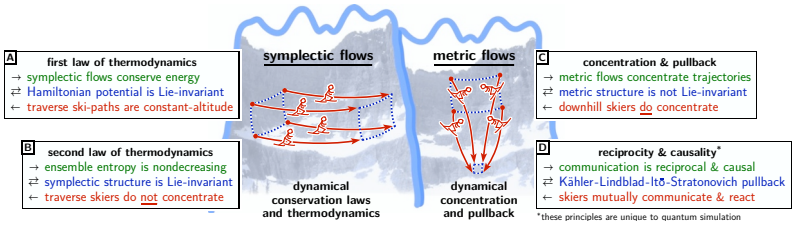

Figure 2 Dynamical processes in spin microscopy are naturally described in terms of symplectic flows (**A**–**B**) that respect thermodynamical laws, and metric flows (**C**–**D**) that describe measurement, control, and noise processes. In consequence of compressive Lindbladian dynamics, numerical trajectory integration is efficient even for systems of hundreds of spins [5].

Emerging Roadmaps and Enterprises As large-scale quantum simulation methods become more efficient, quantum systems engineering methods become more practical; in consequence the present decade is effectively a "Sputnik Moment" for magnetic resonance research and enterprise that is witnessing a "Cambrian Explosion" of diverse experimental methods and theoretical ideas. Our present theoretical and experimental investigations are exploring the physics of polarization transport processes in large magnetic gradients, with a view toward achieving by dynamical nuclear spin polarization an MRFM signal strength sufficient for imaging with $(0.5\,\mathrm{nm})^3$ voxel resolution, sufficient for the direct imaging of (for example) the changes in chromatin architecture that are associated to cell differentiation in regenerative healing processes.

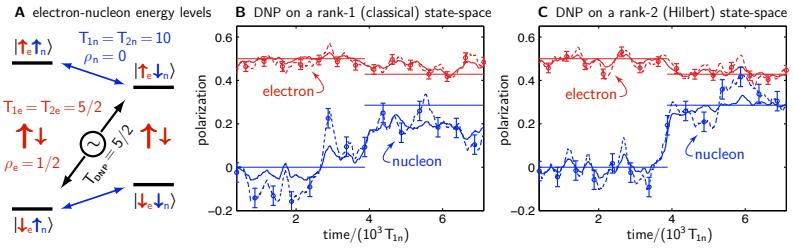

Figure 3 The large magnetic gradients of spin microscopes are a new environment for polarization transport. Novel (and potentially practical) mechanisms for dynamical spin polarization are associated to these gradients [5].

Acknowledgements This work is dedicated to the families of the *Ceremony in Honor of Wounded Marines*, 12 May 2006, Marine Corps Barracks, Washington, DC. This research is supported by the Army Research Office (ARO) under MURI program # W911NF-05-1-0403. Presented as poster #PA-15, 52nd ENC, April 10–15 2011, Asilomar CA.

[1] C. L. Degen, M. Poggio, H. J. Mamin, C. T. Rettner, and D. Rugar. Nanoscale magnetic resonance imaging. *Proc. Nat. Acad. Sci. USA*, 106(5):1313–1317, 2009.
[2] J. Von Neumann. Letter to Norbert Wiener from John von Neumann. In V. Mandrekar and P. R. Masani, editors, *Proceedings of the Norbert Wiener Centenary Congress, 1994*, volume 52 of *Proc. Symp. Appl. Math.*, pages 506–512. AMS, 1997.
[3] J. A. Sidles. Spin microscopy's heritage, achievements, and prospects. *Proc. Nat. Acad. Sci.*, 106(8):2477–8, 2009.
[4] J. A. Sidles, J. L. Garbini, L. E. Harrell, A.O. Hero, J. P. Jacky, J. R. Malcomb, A. G. Norman, and A. M. Williamson. Practical recipes for the model order reduction, dynamical simulation, and compressive sampling of large-scale open quantum systems. *New Journal of Physics*, 11(6):065002 (96pp), 2009.
[5] J. A. Sidles, J. L. Garbini, J. P. Jacky, R. A. R. Picone, and S. A. Harsila. Elements of naturality in dynamical simulation frameworks for Hamiltonian, thermostatic, and Lindbladian flows on classical and quantum state-spaces. *ArXiv e-prints*, July 2010. arXiv:1007.1958.

Spin microscopy's heritage, achievements, and prospects

John A. Sidles[1]

Quantum Systems Engineering Laboratory, School of Medicine, and College of Engineering, University of Washington, Seattle, WA 98195

Achieving 3-dimensional, in-depth, atomic-resolution biological microscopy of undenatured specimens is one of the oldest dreams of science, and for good reason: it unites the thrilling prospect of opening vast new scientific frontiers with cutting-edge technical challenges from every domain of mathematics, science, and engineering.

In a recent issue of PNAS, a team from IBM Research led by Dan Rugar and John Mamin has taken us a giant step closer to this goal (1) by using magnetic resonance force microscopy (MRFM) to obtain 3-dimensional images of tobacco mosaic viruses having voxel resolution down to ≈4 nm. Our comments on the IBM experiment will be modeled on a 1946 letter from John von Neumann to Norbert Wiener (2), in which von Neumann discusses, at considerable length, both the practical problem of achieving atomic-resolution biological microscopy and the potential applications of this capability. Von Neumann's letter invites Wiener to consider whether atomic-resolution biological microscopy might be achieved "by developments of which we can already foresee the character, the caliber, and the duration. And are the latter two not excessive and impractical?"

We adopt von Neumann's question as this commentary's focus, and we seek to describe paths by which mathematicians, scientists, and engineers—of almost every discipline—can contribute to, or benefit from, this centuries-old quest.

We begin by conceiving of spin microscopy in terms of communication: we regard sample spins as being modulated by Alice so as to create a signal force $f(t)$ that is observed by Bob (Fig. 1).

We ask the natural question, how fast can Alice transmit information to Bob? This rate, called the *channel capacity*, is rigorously bounded by Claude Shannon's 1949 Capacity Theorem as

$$C \leq 0.476 \times f_{\rm sig}/(m^2\omega_0^2 S_f S_q)^{1/4}. \qquad [1]$$

The meaning of these parameters and their values in the IBM experiments are as follows: Alice's root-mean-square force signal is $f_{\rm sig} \simeq 10$ aN, Bob's MRFM cantilever has mass $m \simeq 0.26$ ng, frequency $\omega_0/(2\pi) \simeq 2.9$ kHz, force noise $S_f^{1/2} \simeq 10$ aN/$\sqrt{\rm Hz}$ (one-sided), and measurement noise $S_q^{1/2} \simeq 1.0$ pm/$\sqrt{\rm Hz}$. The coefficient 0.476 is the extremum of *Shannon's waterfilling integral* (equation 32 in ref. 4) for $S_{\rm f}$ and $S_{\rm q}$ varied with $S_{\rm f}S_{\rm q}$ held fixed.

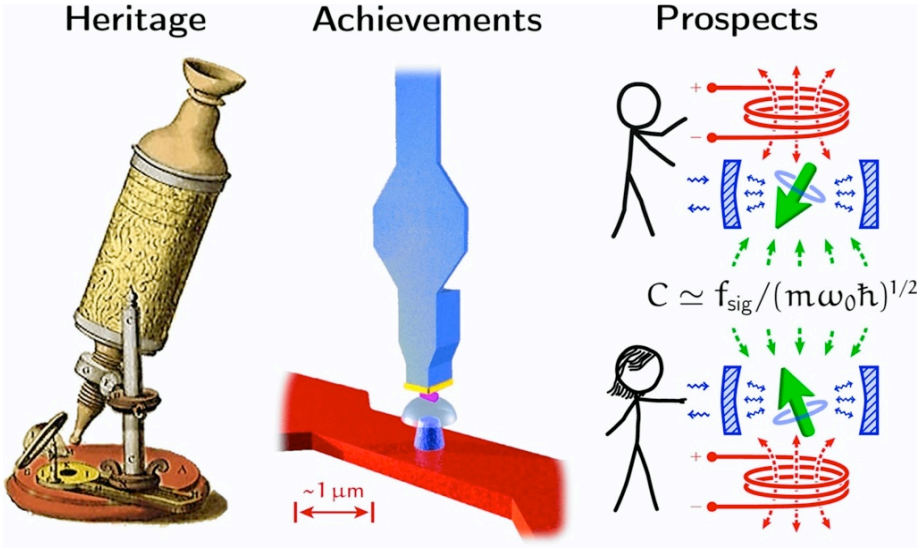

Fig. 1. Spin microscopy continues a heritage that began with Robert Hooke's 1667 vision that (3) "by the help of microscopes, there is nothing so small, as to escape our inquiry" (*Left*). The imaging achievements of the IBM Research Division (*Center*) extend and strengthen this heritage. These achievements lead us to conceive of microscopy as sample spins (Alice, at lower right) transmitting information to observers (Bob, at upper right). With continued advances in nanotechnology, materials science, quantum information science, and many other disciplines—advances that in aggregate are transforming present conceptions of microscopy—Hooke's centuries-old vision may become a twenty-first century reality (Alice and Bob figures by permission of www.xkcd.com).

Inserting these IBM device parameters into Eq. **1**, we compute a capacity bound of $C \lesssim 40$ bits/s. This figure-of-merit, and elaborations of it, will be the main focus of this commentary. Von Neumann and Wiener would recognize this approach as a *Fermi calculation*, and perhaps would be pleased that the methods of their colleague Enrico Fermi are now regarded as essential to design and systems engineering (5).

Multiple paths of inquiry depart from this Fermi calculation starting point. Communication theorists will recognize that a stronger capacity bound is obtained by specifying $S_{\rm f}$ and $S_{\rm q}$ individually, rather than constraining only their product $S_{\rm f}\,S_{\rm q}$ as in Eq. **1**. The resulting expression is more complicated than Eq. **1** (and is not given here) but the bound obtained is not much stronger: $C \lesssim 8.5$ bits/s. This means that the IBM team has balanced force and measurement noise nearly optimally. Good.

Imaging researchers will appreciate that 8.5 bits/s is painfully slow, equivalent to transmitting a 90-kB image file in 24 h. Together with inevitable real-world inefficiencies, this explains the lengthy 120-h acquisition time of the IBM images (1). Slow imaging is a generic challenge in magnetic resonance, and an array of remediating techniques stand ready to be applied, including signal multiplexing, incorporation of ab initio information into modulation and deconvolution algorithms, and (very recently) sparse sampling. Researchers will not soon exhaust these possibilities.

It is good to acquire data faster, so let us now consider paths for boosting the raw channel capacity of Eq. **1**.

Quantum information researchers will recognize that the noise product $S_{\rm f}S_{\rm q}$ is subject to a fundamental (and rigorous) inequality $S_{\rm f}S_{\rm q} \geq \hbar^2$ (one-sided) (equation 6.7 in ref. 6), which is called the *standard quantum limit* (SQL). Eq. **1** then implies the *test-mass capacity bound*

$$C \leq 0.476 \times f_{\rm sig}/(m\omega_0\hbar)^{1/2}. \qquad [2]$$

Author contributions: J.A.S. wrote the paper.

The author declares no conflict of interest.

See companion article on page 1313 in issue 5 of volume 106.

[1]E-mail: sidles@u.washington.edu.

We see that if the noise in the IBM experiment were reduced to its quantum limit, such that $(S_f S_q)^{1/2}$ was reduced from $\approx 3.0 \times 10^4\ \hbar$ to $\approx 1\hbar$, the information flow would increase by ≈170, and the imaging time would drop from 120 h to ≈40 min, which is comparable to traditional imaging methods.

Again, our Fermi calculation illuminates multiple paths of inquiry. Condensed matter physicists will recognize the need to understand the force noise S_f. Sensor scientists will perceive an opportunity to reduce the measurement noise S_q. Nanotechnologists will conceive of lower-mass, sharper-tipped MRFM cantilevers. Spin physicists and chemists will seek to augment signal strength via dynamic polarization. Biologists will appreciate that sample preparation is an immensely challenging and creative scientific discipline in its own right. Again, researchers will not soon exhaust these possibilities.

In the early days of MRFM, it was foreseen that progress in these areas eventually would arrive at atomic-resolution spin microscopy. For example, a 1992 MRFM theory article (7) analyzed a device having (per Eq. **2**) a single-proton quantum capacity bound of ≈3,300 bits/s. Nowadays, this early MRFM vision has not altered much . . . except that the MRFM community has developed a sober appreciation of the immense challenges of approaching quantum limits, in particular, in demonstrating the requisite systems-level innovation and integration. The IBM team has consistently led the world in innovative MRFM systems integration, achieving numerous important milestones such as the first MRFM experiment (8), the first detection of statistical polarization by MRFM (9), the first detection of gradient suppression of spin diffusion (10), the first MRFM detection and imaging of a single (electron) spin (11), and now the first high-resolution MRFM biological images (1).

Let us consider one final Fermi calculation, with a view toward illuminating some of the paths that lie ahead. We notice that an MRFM cantilever and a spin-j particle in a magnetic field both have uniform energy-level spacing, so that an MRFM cantilever can be regarded as a large-j spin. This simple change of variables induces an equivalence $f_{sig}/(m\omega_0\hbar)^{1/2} \leftrightarrow \sqrt{j_B}\ \gamma_B B_A$ [which also follows from quantum simulation theory (12)] under which Eq. **2** becomes a *linearized spin capacity bound*:

$$C \leq 0.476 \times \sqrt{j_B}\ \gamma_B B_A. \qquad [3]$$

Here, j_B and γ_B are the quantum number and gyromagnetic ratio of Bob's receiver spin, and B_A is the rms signal field from Alice's transmitter spin.

Hooke's centuries-old vision may become a twenty-first century reality.

Now we adopt a point of view that would have seemed fantastical to von Neumann and Wiener's generation: we regard Eq. **3** as a literal description of a spin microscope. Suppose, for example, that Bob observes a single electron spin that is acted on at a distance of (say) 25 nm by the 85 pT (rms) field of Alice's single proton. Then, Eq. **3** tells us that the Alice–Bob single-spin channel has a spin capacity bound of ≈5.0 bits/s.

What was a fantastical dream in the twentieth century is becoming a concrete reality in the twenty-first century, thanks to recent work on diamond-spin imaging (13–16) that has greatly expanded our conception of the challenges and opportunities of quantum spin microscopy (17).

Now for the third time our Fermi calculation (Eq. **3**) illuminates multiple paths of inquiry. To cite just one example: the obvious parameter to improve in Eq. **3** is the quantum number j_B. Ought we to begin conceiving of spin microscopes having resonant ferromagnetic receivers with $j_B \simeq 10^6$, for a further 1,000× gain in the capacity bound?

Such possibilities refocus our attention on the key question that von Neumann asked Wiener: Can atomic-resolution microscopy be achieved by developments of which we can already foresee the character, the caliber, and the duration? And are the latter two not excessive and impractical?

The caliber (meaning "size") of the effort is easiest to foresee: the IBM device is comparable in complexity and sophistication to a small earth-orbiting satellite—or to a laser printer. These technologies required a considerable investment in talent and resources to become practical realities, and achieving atomic-resolution spin imaging likely will prove similar. As for the duration of the effort, it likely will be mainly determined by the resources and talent invested in the effort (as with most technologies).

The character of the effort likely will be largely determined by whether quantum theorists and systems engineers can keep up with the experimental physicists. New methods originating in quantum information and simulation theory, in condensed matter physics, and ab initio quantum chemistry are rapidly accelerating the pace and retiring the risks of developing not only quantum spin microscopes, but all technologies that press against quantum limits.

Medical researchers (the tribe to which the author belongs) have aspirations too. We are tantalized by a vision of medical practice becoming fully curative and regenerative. We are frustrated—as the generation of von Neumann and Wiener was frustrated—by the limitations of our present tools. We desire—as Feynman famously desired—to "just look at the thing" (18). And we plan—as every previous generation has planned—for these aspirations to become realities.

ACKNOWLEDGMENTS. This work is dedicated to the families of the *Ceremony in Honor of Wounded Marines*, 12 May 2006, Marine Corps Barracks, Washington, DC.

1. Degen CL, Poggio M, Mamin HJ, Rettner CH, Rugar D (2008) Nanoscale magnetic resonance imaging. *Proc Natl Acad Sci USA* 106:1313–1317.
2. von Neumann J (1997) Letter to Norbert Wiener. *Proc Symp Appl Math* 52:506–512.
3. Hooke R (1665) *Micrographia* (Royal Society, London).
4. Shannon C (1949) Communication in the presence of noise. *Proc Inst Radio Eng* 37:10–21.
5. Magrab EB (1997) *Integrated Product and Process Design and Development* (CRC Press, Boca Raton, FL), pp 112.
6. Braginsky VR, Khalili FY (1992) *Quantum Measurement* (Cambridge Univ Press, New York), pp 79.
7. Sidles JA, Garbini JL, Drobny GP (1992) The theory of oscillator-coupled magnetic resonance with potential applications to molecular imaging. *Rev Sci Instrum* 63:3881–3899.
8. Rugar D, Yannoni CS, Sidles JA (1992) Mechanical detection of magnetic resonance. *Nature* 360:563–566.
9. Mamin HJ, Budakian R, Chui BW, Rugar D (2003) Detection and manipulation of statistical polarization in small spin ensembles. *Phys Rev Lett* 91:207604.
10. Budakian R, Mamin HJ, Rugar D (2004) Suppression of spin diffusion near a micron-size ferromagnet. *Phys Rev Lett* 92:037205.
11. Rugar D, Budakian R, Mamin HJ, Chui BW (2004) Single spin detection by magnetic resonance force microscopy. *Nature* 430:329–332.
12. Sidles JA, *et al.* (2008) Practical recipes for the model order reduction, dynamical simulation, and compressive sampling of large-scale open quantum systems. *New J Phys*, in press.
13. Degen CL (2008) Scanning magnetic field microscope with a diamond single-spin sensor. *Appl Phys Lett* 92:243111.
14. Balasubramanian G, *et al.* (2008) Nanoscale imaging magnetometry with diamond spins under ambient conditions. *Nature* 455:648–651.
15. Maze JR, *et al.* (2008) Nanoscale magnetic sensing with an individual electronic spin in diamond. *Nature* 455:644–647.
16. Taylor JM, *et al.* (2008) High-sensitivity diamond magnetometer with nanoscale resolution. *Nat Phys* 4:810–816.
17. Romalis M (2008) Applied physics: Virtues of diamond defects. *Nature* 455:606–607.
18. Feynman RP (1992) There's plenty of room at the bottom. *J Microelectromech Sys* 1(1):60–66.